




Deployable Soft Origami Modular Robotic Arm With Variable Stiffness Using Facet Buckling

MinJo Park , Woongbae Kim, Sung-Yol Yu, Jungmin Cho, Wonkyeong Kang, Junghwan Byun, Useok Jeong , *Member, IEEE*, and Kyu-Jin Cho , *Member, IEEE*

Abstract—Robots that share activity spaces or physically interact with humans typically benefit from appropriate payload capacity, extensible workspace, low weight, safety, and space efficiency. The soft origami design and mechanism can meet many of these beneficial factors; however, achieving a high payload capacity remains challenging. In this letter, we developed a soft origami arm module with high variable stiffness (x300) and spatial efficiency (compressed x3.1). The buckling of facets into a cylindrical tube followed by its pressurization enables the arm to be highly stiffened. High-pressure capacity was obtained via the sewing-heat press fabrication process. We used a pneumatic pressure–tendon pair and utilized the frictional force between origami and tendon to prevent unintentional gravity-induced deformation while deploying. An analytical model was developed and compared to the experimental results. With our modular design, we could easily build functional robotic structures. Two robotic demonstrations were performed to examine the expandability of the modules. A variable-length robotic arm that mimics a human arm was built to manipulate typical objects. Additionally, a soft cover, which could carry 14 kg of weight and change its volume 29 times for improved spatial efficiency, was developed. This research suggests a new design methodology for practical soft robotic systems.

Index Terms—Origami, soft robot applications, soft robot materials and design, variable stiffness.

Manuscript received 2 September 2022; accepted 13 December 2022. Date of publication 26 December 2022; date of current version 10 January 2023. This letter was recommended for publication by Associate Editor D. Aukes and Editor Yong-Lae Park upon evaluation of the reviewers' comments. This work was supported in part by The Ministry of Trade, Industry and Energy (MOTIE), Korea, under Grant 20008908 and in part by the National Research Foundation of Korea (NRF) funded by the Korean Government (MSIT) under Grant NRF-2016R1A5A1938472. (*Corresponding author: Kyu-Jin Cho.*)

MinJo Park, Sung-Yol Yu, Jungmin Cho, Wonkyeong Kang, and Kyu-Jin Cho are with the Biorobotics Laboratory, Soft Robotics Research Center, Department of Mechanical Engineering, Institute of Engineering, Seoul National University, Seoul 08826, Republic of Korea (e-mail: mjpark1995@gmail.com; joseph.yu2013@gmail.com; jungmin97@snu.ac.kr; wk000106@snu.ac.kr; kj-cho@snu.ac.kr).

Woongbae Kim is with the Biorobotics Laboratory, Soft Robotics Research Center, Department of Mechanical Engineering, Institute of Engineering, Seoul National University, Seoul 08826, Republic of Korea, and also with the Artificial Intelligence and Robotics Institute, Korea Institute of Science and Technology, Seoul 02792, Republic of Korea (e-mail: wbae2022@kist.re.kr).

Junghwan Byun is with the Physical Intelligence Department, Max Planck Institute for Intelligent Systems, 70569 Stuttgart, Germany (e-mail: yongsamari@snu.ac.kr).

Useok Jeong is with the Robotics R&D Department, Korea Institute of Industrial Technology, University of Science and Technology, and HYU-KITECH, Ansan-si 15588, Republic of Korea (e-mail: snopyy86@gmail.com).

This letter has supplementary downloadable material available at <https://doi.org/10.1109/LRA.2022.3232267>, provided by the authors.

Digital Object Identifier 10.1109/LRA.2022.3232267

I. INTRODUCTION

THE prominent aspects of current robotics technology are space sharing and physical interaction with humans [1], [2]. Therefore, the concepts of payload, workspace, safety and space efficiency are no longer separate factors and should be considered together in robot design. In the last decade, considerable efforts have been made to meet these essential factors [3]. However, some of them conflict with each other; for example, lightweight and miniaturized designs improve safety but limit the payload capacity and workspace [4].

Soft deployable robots, made of low-rigidity materials such as fabric, film, and polymer, are light, safe, and can change their own body length, allowing space-efficient robot designs to cover larger workspaces [5], [6]. However, the low weight and safety factor hinder their ability to withstand high external loads. For example, growing vine robots that comprise thin membranes and elongate through eversion of body actuated by internal pressure were proposed to perform various tasks such as delicate manipulation, cooperating with humans, and exploring confined space [7]. However, their inherent mechanism, which requires all the parts of the body to be rolled into a base and deformed significantly through an eversion process, limits the thickness and stiffness material, and consequently, hinders its ability to withstand high external forces.

Origami robots have been actively studied for use in deployable structures [8], [9]. Owing to the kinematics of the origami patterns, some origami tube structures can effectively generate linear motions with high deployment ratio [10], [11], [12]. Similar to vine robots, lightweight origami tube composed of flexible sheet material with an empty interior enables safe interaction with humans. However, unlike the vine robots that undergo large deformation throughout the entire body, the origami robots undergo local deformation mainly on the crease lines and can be designed with relatively stiff materials, thick structures, and appendages. Variable stiffness mechanisms of origami robots have been developed for practical real-world tasks that require large payloads. The addition of stiffening components such as shape memory polymer alloy (SMA) [13] or jamming (granular [14], layer [15]) gives rise to issues related to control, fabrication, and integration complexity. Owing to the simple control of sealed origami structures, they are pressurized for actuation and stiffening of the soft structure [16], [17]. However, the pressurization method for the origami tubes has some limitations. First, excessive increase in pressure will cause the facets and crease lines to deform toward out-of-kinematics configurations, resulting in structural failure. Second, pneumatic origami robots have vulnerable “sealing regions” to which sealing solutions such as adhesive tape, polymer coating, and thermoplastic heat

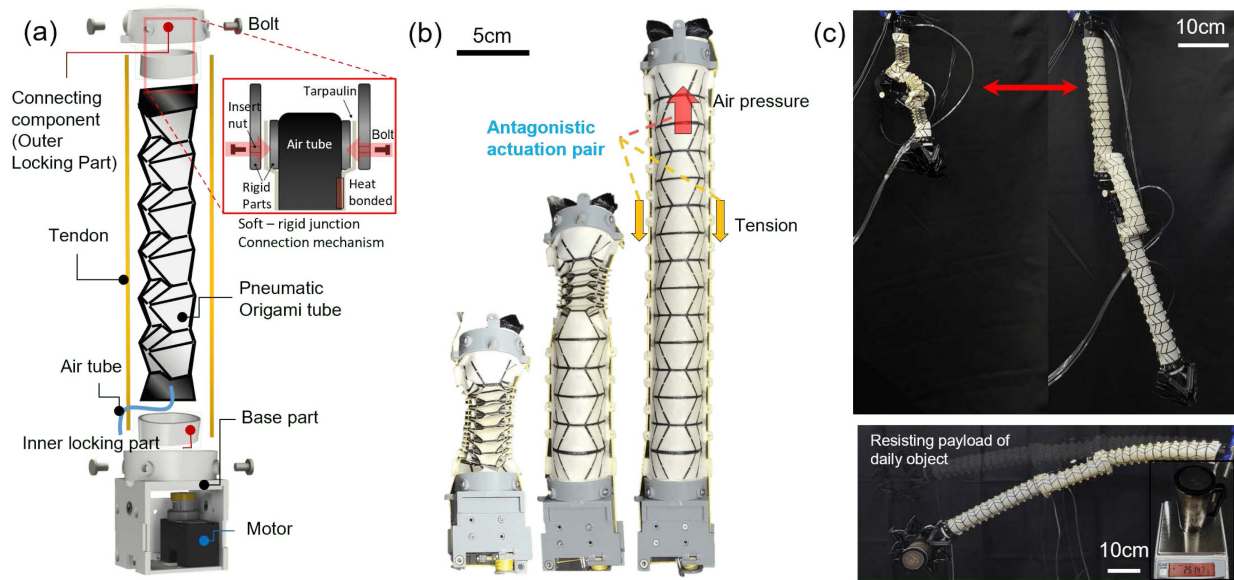


Fig. 1. A soft origami arm system (a) Components of the module (b) A deployment process of the module (c) A demonstration of the proposed arm.

bonding have been applied. To extend the performance of the soft origami structure, high operation pressure and structural stability must be ensured.

In addition, complex real-world tasks, such as carrying bulky and heavy objects and manipulating them at a meter scale, pose important challenges in soft robotics applications. Soft robot systems should have a sufficient degree of freedom and should be properly configured to manage complicated and sequential tasks. Unlike conventional top-down design approaches, which focus on unique structures, a modularized design, which is a bottom-up approach for designing versatile robotic systems [18] through assembling, and disassembling processes can be an appropriate method. However, previous soft modular robots cannot withstand kilogram scale load, designed for recombination and air connection. The modulus difference between the rigid connecting parts and soft materials makes it challenging to create a robust junction. Therefore, a new concept of a soft arm module that can be highly stiffened and has a robust connection between modules for real-world tasks is required.

In this letter, we propose a novel concept of a soft origami robot arm module with a wide range of bending stiffness (up to 300 times) and expandability for various target functions of robotic systems. Our main contributions are as follows: (1) To achieve a wide stiffness range, we employed facet buckling and pressurization of the soft origami tube and validated the effectiveness of the buckling. (2) A new sewing-heat press method that maintains air tightness even under high pressure (300 kPa) was developed. (3) We prevented unintentional gravity-induced bending of pneumatically actuated soft origami in the deployment process by utilizing a tendon and the frictional force between origami and tendon. (4) We introduced the simple modular concept for origami to achieve complex robotic applications. To validate the performance of the origami arm module, various experiments were conducted for measuring the bending stiffness, and a bending model of the buckled origami tube was developed. To manage high cohesion at the junction between

soft origami and rigid connecting part, a mechanical-jamming locking mechanism was developed. To evaluate this modular concept, two different robotic applications were conducted for real-world human-scale applications. We built a robot arm (356 g) with a high moment arm (90 cm) and demonstrated successful manipulation of daily objects (<250 g). Additionally, a new soft rover was developed, which deployed from an initial small volume state (29 times volumetric change) and stiffened to carry heavy cargo (14 kg).

II. DESIGN OF THE SOFT ARM MODULE

A. Concept and Design Parameters

Fig. 1 shows the concept and overall structure of the soft origami arm. It is capable of changing its length through reversible linear motion with a high deployment ratio, and functions as an “arm” to manipulate the objects. To design a soft arm, we utilized a Tachi-Miura origami pattern (Fig. 2(a)) [19]. Tachi-Miura satisfies the requirements of high stiffness and high deployment ratio because it deforms to a cylindrical shape in high pressure and has 1-DOF these are advantageous for the linear deploying motion and can be flattened to 2D for fabrication. The Tachi-Miura origami pattern has several design parameters, such as the length and angle of the trapezoid (l_1), parallelogram (l_2), right triangle (l_3), angle (θ), and crease line width (t). The total width ($l_1 + l_2 + l_3$), angle (θ), and crease line width (t) are the important factors that determine the size, deployment ratio, and stiffness, respectively. Considering the deployment speed related to the flow rate, a 60 mm width was chosen and the base length of each figure was equally spaced. Additionally, regarding the angle stability and deployment ratio, there are trade-off issues. Due to the thickness of the origami, the large angle increases the deployment ratio; however, it inhibits contracting motion because it induces movement toward the deployed zero-volume state. So we chose the angle of 60° for the balance of folding stability and deployment ratio.

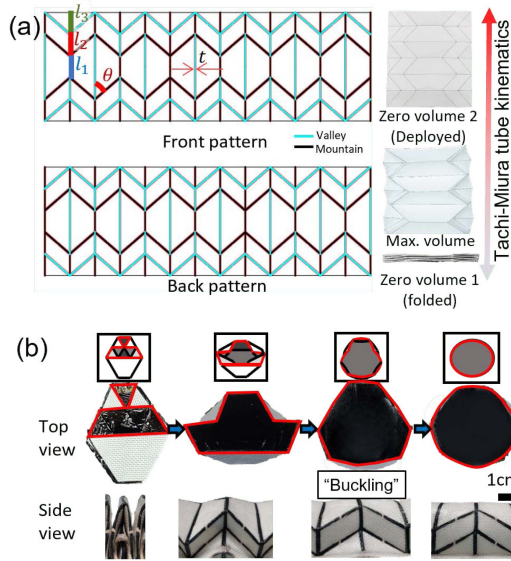


Fig. 2. Parameters and a stiffening principle (a) A Tachi-Miura origami pattern and parameters (b) The facet buckling as pressure increasing.

B. Design Principle

In the soft robotic system, especially over tens of centimeters large scale, achieving the wide-range bending stiffness and preventing bending during deployment have been challenging [20]. To solve this problem, we exploited the buckling of origami induced by air pressure, and the pneumatic pressure-tendon pair for the stable deployment. As the internal pressure increases (Fig. 2(b)), the facets and crease lines are deformed to curvy shapes and, finally, a perfect cylindrical shape is achieved. In a previous letter, the buckling phenomenon was analyzed well at every vertex [21]. Due to the buckling effect, a higher bending stiffness could be obtained as the cross-section approaches the circular shape. Therefore, our soft arm could be highly stiffened. Also, to manage complex and sequential real-world tasks, the soft robotic system must have the proper structure suitable for the target mission. However, tackling the target function through designing and making a single soft structure each time required significant effort and trial and error. Using a modular concept makes it possible to design an appropriate soft robot system by connecting each module. Thus, the rearrangement mechanism of the module, similar to block toys, could be achieved. However, the modulus difference, which induced stress concentration at the junctions, made it challenging to achieve a strong-detachable connection between the soft and rigid parts. As a solution, we designed a mechanical jamming-locking mechanism. Attaching and detaching processes were simple and the coherence could be increased by applying the higher normal force. We inserted the extended part of the soft actuator (Tarpaulin) between the outer locking and Inner locking parts, and then fastened them using insert nuts and bolts. With this mechanism, the separation between the soft and rigid parts was completely prevented, and a tight connection was also formed. (inset, Fig. 1(a))

III. FABRICATION

For rapid and simple fabrication, SCM (Smart Composite Microstructure) method is the proper way of building the

Tachi-Miura soft origami arm. In the fabrication of a pneumatic origami structure, the robust sealing process at crease lines and vertex points has been challenging and time-consuming. In the previous studies, the air tightness was secured with an additional sealing material such as a separate driving balloon inside the origami shell [22], coating the outside with silicone rubber [23], [24], or applying adhesive tape to seam [25], [26], [27]. However, the operating pressure ranges of the origami structures from previous studies were insufficient to secure high bending stiffness. As a solution, a ‘‘Sewing - Heat press’’ method was developed in this letter to withstand high pressure (300 kPa). Fig. 3 shows the overall fabrication process, and the details are as follows:

- 1) 15um-Kapton sheet (15 um), 100 um-TPU sheet (NASA-T, Sambu Fine Chemical), 50 um-Ripstop-Nylon fabric, and 400 um-Tarpaulin (GUANGZHOU YUXIN PLASTIC) are cut using a laser cutter and the crease pattern and tendon rings were formed.
- 2) Sheets are stacked and sewed using a sewing machine (Zuki, DDL-9000 C) following the closed-rectangular path to form an inner tube.
- 3) Tarpaulin and additional TPU sheets are heat pressed with the inner tube at 500 kPa and 170° for 1 h. In this step, TPU permeated into Nylon fabric and formed black crease patterns.
- 4) After cooling, a Polyurethane tube was connected to a flattened Tachi-Miura tube and the sealing adhesive (Permabond 2050) was applied.
- 5) A flat structure is weakly folded by hand to induce the mountain-valley pattern and vacuumized to form a precise Tachi-Miura configuration in an oven at 90° for 20 min.

By sewing and heat pressing with additional TPU, the TPU permeated and hardened into the nylon fabric and sewn area. The sewing thread and the nylon fabric acted as reinforcing mesh for the TPU chamber, increasing the operating pressure. In the oven process, a mountain, valley pattern of origami was formed by the glass-transition of the TPU, so that the initial state of the origami shifted to a folded zero volume state and memorized its configuration with a small deviation (Fig. 3(d)). A tensile test was conducted to validate the effect of sewing. Sewing and heat bonding were applied to one sample, and another one was bonded using only heat bonding. A comparison of the maximum stress in the two cases revealed a difference of 4 to 5 times with or without sewing. Since the origami arm was composed of thin sheets, the 31 cm arm weighed only 43 g. Therefore, due to its small momentum when the arm moves, safety would be increased in the situation that contact with the external environment. Additionally, the length could be varied from 10 cm to 31 cm, so it could be that the spatial efficiency in an idle state could be increased. The final step was integration with the motor (Robotis, XL330), tendon (PE), and 3D-printed connection parts (Prusa Mk3, PLA). Rigid parts were tightly attached using the ‘‘connection mechanism’’ at each side of the soft link. To actuate the soft origami link, the far side connecting component and motor were connected by the tendon.

IV. ACTUATION MECHANISMS AND CONTROL

We developed a ‘‘Sequential deployment mechanism (Fig. 4(b), (c))’’ for stable deployment. The origami unfolding process started at the lowermost layer because the sum of frictional drag between the tendon ring and the tendon can

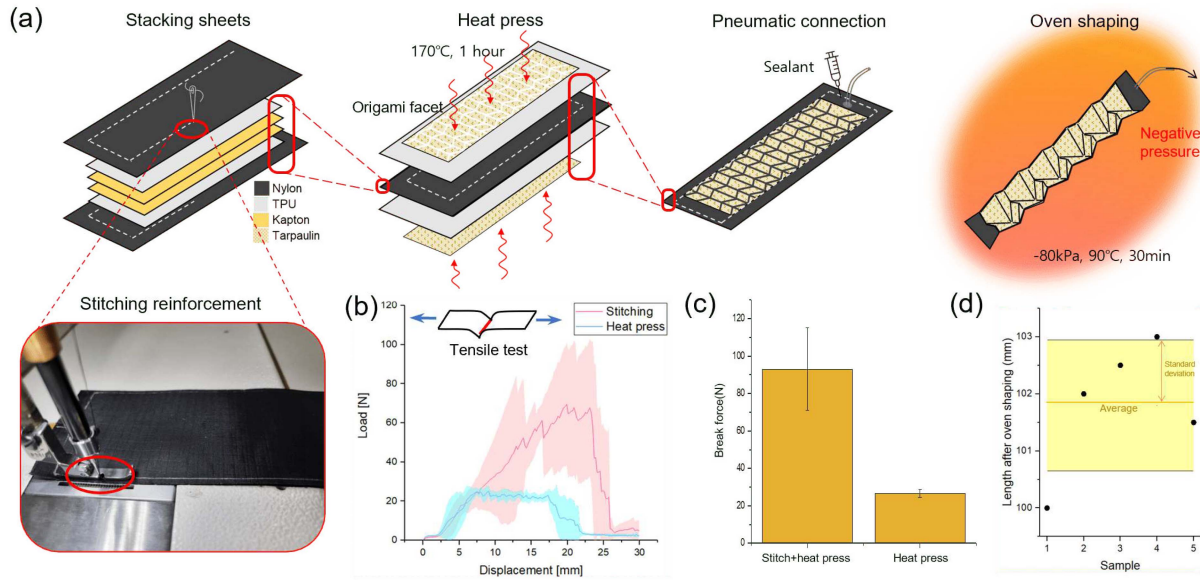


Fig. 3. A fabrication of the origami arm (a) Fabrication steps (b) Tensile tests (c) A result of the tensile tests (d) The repeatability of the oven-shaping process.

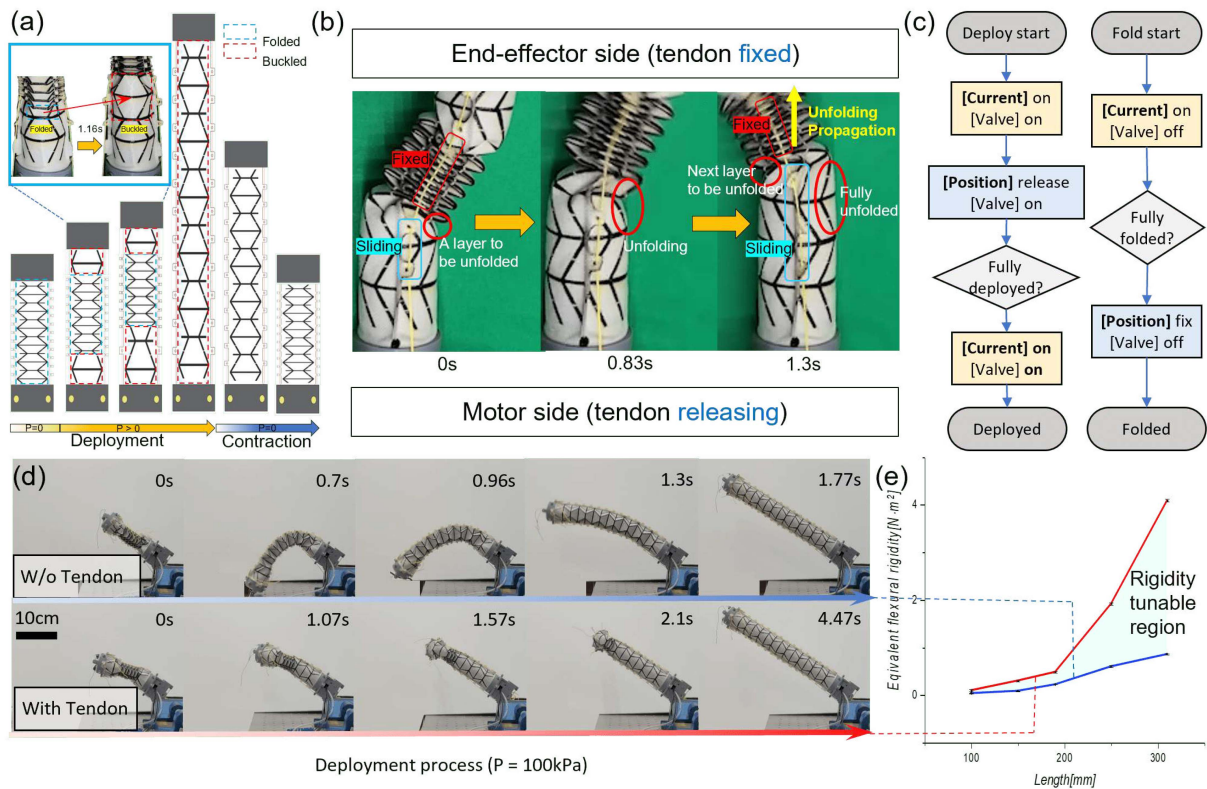


Fig. 4. An actuation mechanism (a) The sequential deployment and contraction process (b) A side view of the one-layer unfolding process (c) Control block diagrams (d) An effect of tendon actuation (e) Two deployment paths and the possible rigidity-length region.

be minimized by following that path. The other layers could not be unfolded, because if so, more tendon rings engaged in slip, creating more friction, and the total resistance was greater than when the bottom part was unfolded. The same process was continuously repeated on the adjacent upper layer after the below layer was fully inflated. Finally, when all the layers were

fully deployed, the shape of the arm was fixed to a cylindrical column. A block diagram of the controlling mechanism was shown in Fig. 4(c). When the command started the deployment process from the initial folded state, the valve was opened and pneumatic pressure was applied to the origami tube. Then, the length of the tendon was increased by controlling the position of

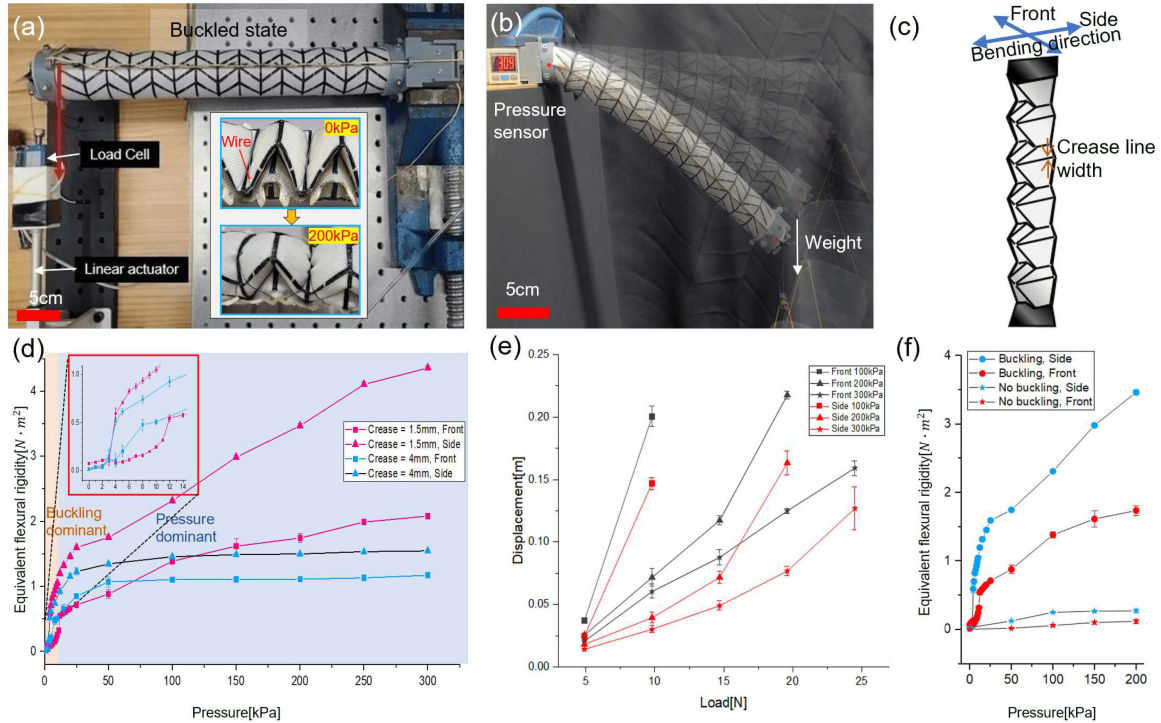


Fig. 5. Bending stiffness experiments (a) A bending test setup (b) A large deformation test setup (c) Parameters of the bending test (d) A Result of the bending test (e) A result of the large deformation test (f) An effect of buckling on the equivalent flexural rigidity.

the motor. When the arm reached the maximum length, the mode changed to pull the tendon with a constant force. To contract the arm, the valve reduced the pressure and volume inside the origami. Then, the buckled origami arm returned to its original Tachi-Miura shape by a restoring force generated in the oven shaping process. Simultaneously, the tendon was contracted through the current control for stable folding of the arm. At each length, Pressure could be highly increased during the deployment process because the tendon limited the longitudinal elongation by the pressure, making pressurization and deployment independent. As a result, straightened deployment following the upper path in Fig. 4(e) (red line) was possible. In the absence of tension, the arm reached the maximum length at low pressure (< 20 kPa).

As a result, sufficient stiffness could not be generated, following the lower path in Fig. 4(e) (blue line). We defined equivalent flexural rigidity (EFR), to quantify the flexural rigidity of the nonuniform origami arm in an axial direction. We measured EFR using the same setup in Fig. 5(a).

$$EFR = \frac{PL^3}{3\delta} \quad (1)$$

(P: bending force, L: Length of arm, δ : displacement)

V. BENDING STIFFNESS EXPERIMENT AND ANALYSIS

To measure the bending stiffness of the origami arm, a load cell was fixed to the linear actuator, and the other end was connected to the arm with a thread. Pulling force-displacement relationships were obtained for various lengths (10–31 cm) and pressure (0 kPa–300 kPa). Since the arm had an anisotropic geometry, experiments were conducted in the front and side

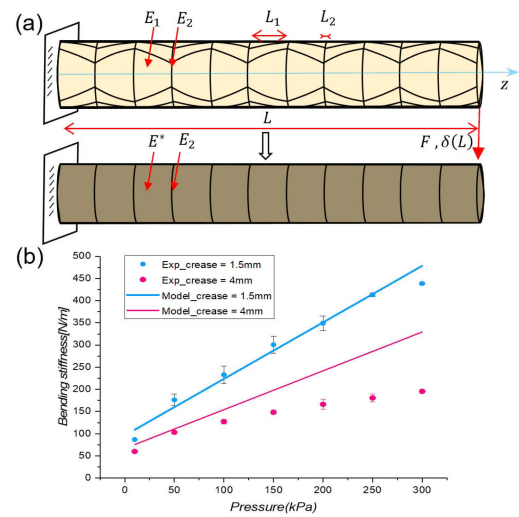


Fig. 6. Modeling (a) A simplified model of the arm (b) A modeling result.

pulling directions (Fig. 5(c)). Furthermore, two types of arms that had different crease line widths (1.5 mm, 4 mm) were tested.

As a result, with the increase in pressure, the arm stiffness could be modulated up to 300 times. Additionally, according to the pressure range, two different stiffness slope patterns were observed. The bending stiffness in the low-pressure region (0 kPa–12 kPa) increased very rapidly compared to that of the high-pressure region (> 20 kPa). The buckling process ended before the pressure increased by less than 2–4 kPa. As buckling was completed, the arms were locked in a cylindrical shape

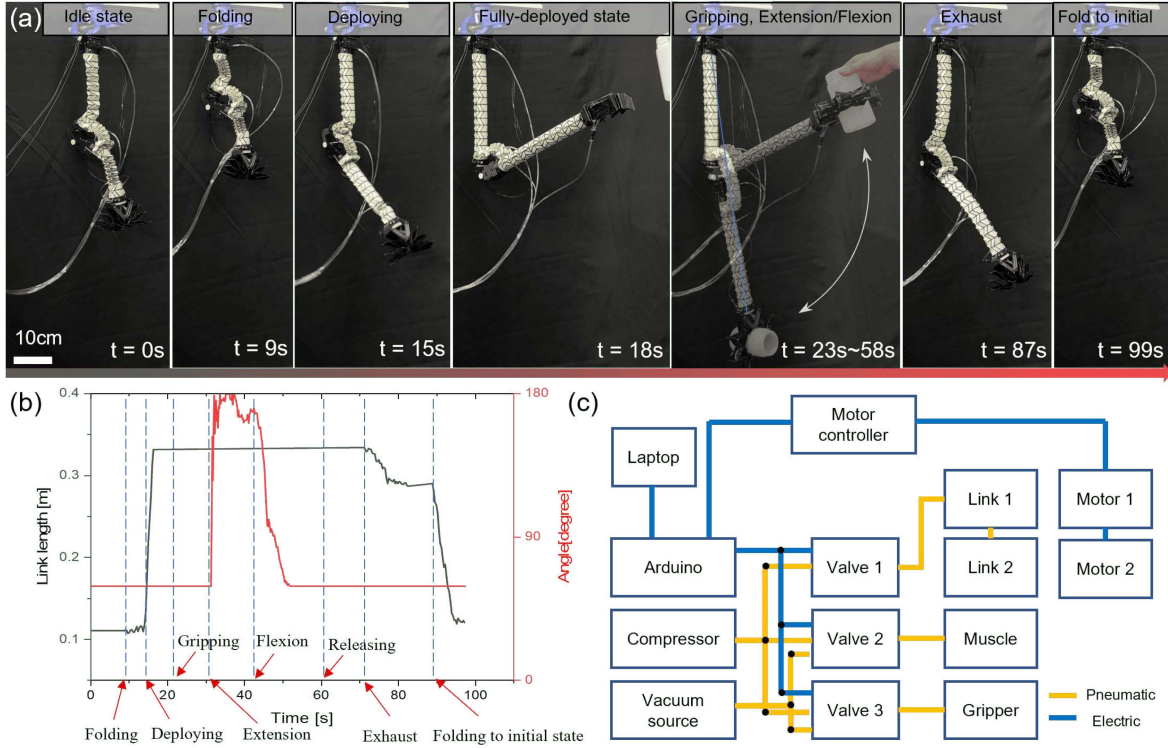


Fig. 7. A demonstration of the robotic arm (a) A working process of soft robotic arm (b) Kinematics of the arm (c) A schematic of the actuation system.

and the stiffness increased slowly (Fig. 2(d)). The stiffness increment in the buckling dominant region accounted for roughly 20%–40% of the full range stiffness increments. In addition, we validated the effect of the buckling by preventing buckling with the thread even at high pressure (Fig. 5(a)(inset), (f)). At 200 kPa, the EFR of the buckled state is 12–14 times higher than the not buckled state. Therefore, it could be concluded that the buckling phenomenon significantly contributed to the stiffening of the arm. Compared to the 1.5 mm arm, the arm with a wider crease line (4 mm) had a low bending stiffness increment. This was a predictable result because more soft and thin regions make the structure flexible. Also, the large deformation of the arm under a large load (0.5 kg~2.5 kg) was analyzed by applying the gravitational torque (Fig. 5(b), (f)).

VI. MODELING

To model the bending stiffness of the soft origami arm (Fig. 6), analysis was performed by assuming that the fully-deployed arm acts as a cantilever beam, and the point load is applied to the end of the arm. On the z-axis, the part where crease lines and facets are mixed and the part where crease lines only exist appeared repeatedly. We assumed that the mixed part can be replaced with a uniform material by averaging the flexural rigidity. As a result, the origami arm could be simplified to be patterned by alternating materials with two different flexural rigidity. An analytic solution for a simplified origami arm was derived through Euler's beam bending theory. The Young's modulus of the fabric is increased when the internal pressure increases, so we linearized Young's modulus-pressure relationship using the result of the previous studies [28], [29]. Moreover, the additional modulus term due to the pressure stiffness was

simply added to modulus value [30]. The analytic solution of the load-displacement relationship is as follows.

$$\delta(L) = \frac{FL_1^3(n+1)^3}{3E^*I_1} + \frac{FL_1^2L_2n(n+1)(4n+1)}{6E^*I_1} + \frac{FL_1L_2^2n(n+1)(2n+1)}{6E^*I_1} + \frac{FL_2^3n^3}{3EI_2} + \frac{FL_2^2L_1n(n+1)(4n-1)}{6EI_2} + \frac{FL_2L_1^2n(n+1)(2n+1)}{6EI_2} \quad (2)$$

(L_1 : length of the patterned region, L_2 : length of the crease line, n : number of the repeated patterns, L : total length, E^*I_1 : equivalent flexural rigidity of the patterned region, EI_2 : flexural rigidity of the crease line) In general, the length of the facet region is much larger than that of the crease line in most origami, so we could eliminate the high order terms of L_2 in equation (1). Equation (1) can be approximated as equation (2).

$$\delta(L) = \frac{FL_1^3(n+1)^3}{3E^*I_1} + \frac{FL_2L_1^2n(n+1)(2n+1)}{6EI_2} \quad (3)$$

The first term is related to the stiffness of the facet region and the second term is related to the crease line characteristic. As the ratio of the area ($A_{crease\ line}/A_{facet}$) increases, the rate of modulus changing by fabric pressurization decreases; thus, lowering the gradient of the bending stiffness-pressure graph. In real experiments, the buckling was induced at crease lines. As the crease line width increased, larger buckling occurred. Therefore in Fig. 6(b), larger crease line

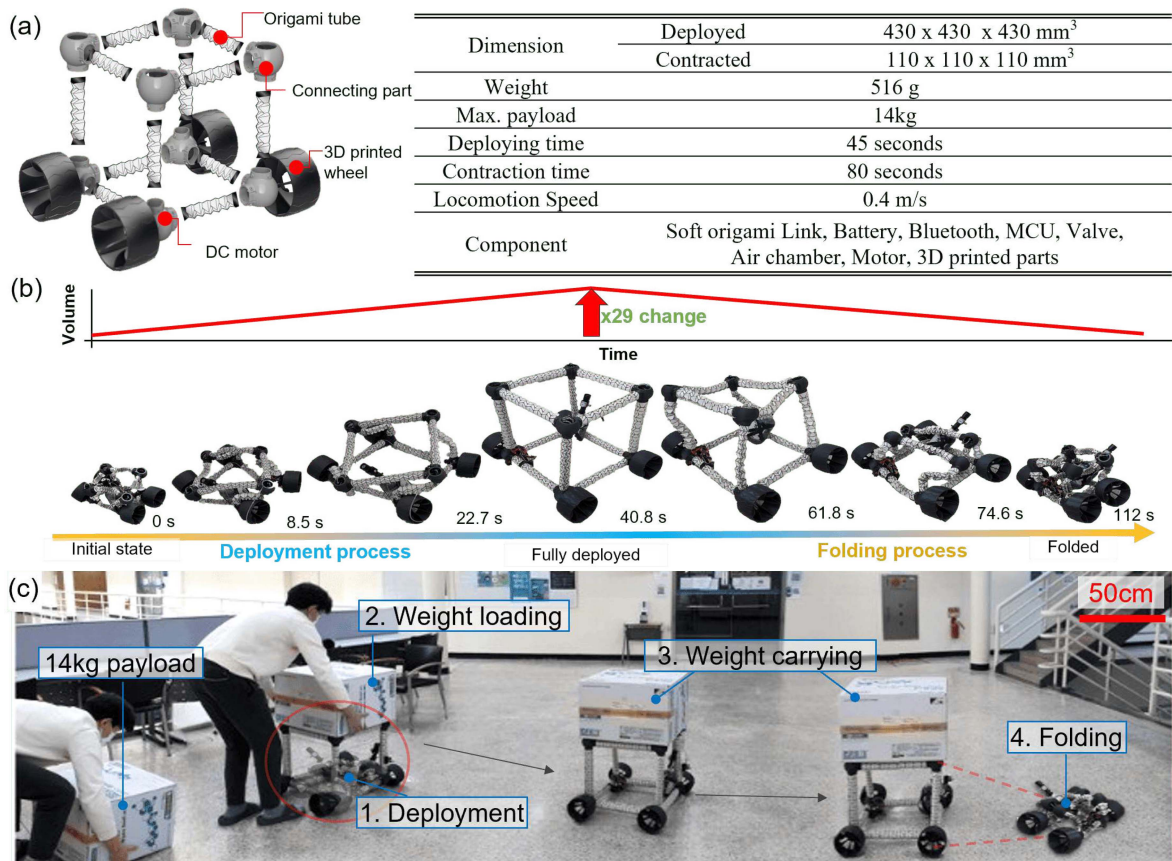


Fig. 8. A high-payload deployable soft rover (a) Main components of the rover (b) Deployment and folding processes (c) A weight-carrying demonstration.

width had larger error values. Moreover, the boundary condition at the base part was not perfectly fixed like a cantilever beam, resulting in slight differences between the modeling and experiments.

VII. APPLICATION

A. Deployable Robotic Arm

The developed soft origami arm was safe and had spatial efficiency, so it could be applied to the real robotic arm that shares space with humans. To demonstrate its potential, we developed a soft robotic arm that mimics a human arm to manipulate daily objects. The soft robotic arm consisted of two origami arm modules. We designed a free-rotating joint that connected two arm modules. We inserted a 3D-printed column into the holes of the connecting parts to form the rotating joint. To change the angle between the upper arm and lower arm, an additional soft module was integrated into the rotating joint, which served as biceps for flexion (negative pressure) and triceps for extension (positive pressure). In addition, we attached a deployable gripper at the end of the arm. In Fig. 7, the soft robotic arm was actuated sequentially to perform a simple task. The system was composed of three solenoid valves, a compressor, a vacuum source, and controlling electronics. Because of the deployable structure, the range of motion was increased from 25 cm to 74 cm. Moreover, the arm could be bent by 120° from the straightened configuration.

B. Soft Rover

We presented another potential application “High-payload deployable soft rover” with the proposed arm. Considering the transportation cost and energy efficiency in the exploration process, the lightweight design of the rover had significant advantages. It could absorb shocks in collision with the external environment, especially with humans, because of the inherent softness of the origami tube. In addition, It could be transported efficiently because of its initial small volume and lightness. The proposed rover consists of 12 soft origami modules, one air source, 3D printed connection parts, four motors, one Arduino, and other electronics. All modules are internally connected with the tubes. Due to the deployment behavior of the soft origami arm, its volume can be increased 29 times. The total weight of the soft cubic structure is only 516 g, but the load capacity of the rover is over 14 kg. Reversible and repetitive deployment and contraction processes were possible.

VIII. CONCLUSION

This letter introduces the concept of a deployable soft pneumatic origami arm. By exploiting 1 DOF kinematics of the Tachi-Miura pattern, the arm can be deployed or retracted in the axial direction. In the fabrication step, we developed the “sewing-heat press” and “oven shaping” processes to obtain a robust pneumatic origami structure and generate a resilient force, respectively. The developed soft arm had a high deployment ratio and lightweight characteristics. Additionally,

unintentional deformation during the deployment process was prevented through the “Sequential deployment mechanism”. To quantitatively analyze the soft arm, we measured the bending stiffness at various lengths and pressures, while varying the direction and crease line width. As a result, the equivalent flexural rigidity was modulated up to 300 times in a fully deployed state. During the process, the buckling of the origami was utilized to increase the bending stiffness and we validated the effectiveness of the buckling. For the real-world application, we demonstrated the soft robotic arm and the high-payload carrying soft rover. In future work, a detailed analysis of facet buckling will be conducted. The stiffness difference between buckled origami and inflated tube without crease patterns should be analyzed. If the modulus and thickness of sheets are changed, the buckling behavior and stiffness-pressure relationship will also change to adequately shift the absolute stiffness range. Also, our follow-up research will be conducted on how to use tension to stiffen and maneuver the origami arm with various tendon paths. By using other fabrication machines such as a roller heat press machine or a larger heat presser, we will be able to build much larger scale arms of a meter scale. When the scale changes, it will be necessary to adjust the thickness and physical properties of the origami for a stable actuation.

REFERENCES

- [1] I. Matsuo et al., “Q-bot: Heavy object carriage robot for in-house logistics based on universal vacuum gripper,” *Adv. Robot.*, vol. 34, no. 3/4, pp. 173–188, 2020.
- [2] C.-A. Smarr, A. Prakash, J. M. Beer, T. L. Mitzner, C. C. Kemp, and W. A. Rogers, “Older adults’ preferences for and acceptance of robot assistance for everyday living tasks,” *Proc. Hum. Factors Ergonom. Soc. Annu. Meeting*, vol. 56, no. 1, pp. 153–157.
- [3] T. B. Sheridan, “Human-robot interaction,” *Hum. Factors*, vol. 58, no. 4, pp. 525–532, 2016.
- [4] A. De Santis, B. Siciliano, A. De Luca, and A. Bicchi, “An atlas of physical human-robot interaction,” *Mechanism Mach. Theory*, vol. 43, no. 3, pp. 253–270, 2008.
- [5] W. Kim et al., “Bioinspired dual-morphing stretchable origami,” *Sci. Robot.*, vol. 4, no. 36, pp. 1–11, 2019.
- [6] N. S. Usevitch, Z. M. Hammond, M. Schwager, A. M. Okamura, E. W. Hawkes, and S. Follmer, “An untethered isoperimetric soft robot,” *Sci. Robot.*, vol. 5, no. 40, pp. 1–15, 2020.
- [7] E. W. Hawkes, L. H. Blumenschein, J. D. Greer, and A. M. Okamura, “A soft robot that navigates its environment through growth,” *Sci. Robot.*, vol. 2, no. 8, pp. 1–8, 2017.
- [8] J. Santoso and C. D. Onal, “An origami continuum robot capable of precise motion through torsionally stiff body and smooth inverse kinematics,” *Soft Robot.*, vol. 8, no. 4, pp. 371–386, 2021.
- [9] W. Kim, J. Eom, and K.-J. Cho, “A dual origami design that enables the quasisquential deployment and bending motion of soft robots and grippers,” *Adv. Intell. Syst.*, vol. 4, no. 3, 2022, Art. no. 2100176.
- [10] Z. Zhang, W. Fan, G. Chen, J. Luo, Q. Lu, and H. Wang, “A 3D printable origami vacuum pneumatic artificial muscle with fast and powerful motion,” in *Proc. IEEE 4th Int. Conf. Soft Robot.*, 2021, pp. 551–554.
- [11] J. A. Faber, A. F. Arrieta, and A. R. Studart, “Bioinspired spring origami,” *Science*, vol. 359, no. 6382, pp. 1386–1391, 2018.
- [12] K. Zhang and K. Althoefer, *Designing Origami-Adapted Deployable Modules for Soft Continuum Arms*. Berlin, Germany: Springer, 2019.
- [13] J. Kim, D. Y. Lee, S. R. Kim, and K. J. Cho, “A self-deployable origami structure with locking mechanism induced by buckling effect,” in *Proc. IEEE Int. Conf. Robot. Automat.*, 2015, pp. 3166–3171.
- [14] Y. Li, T. Ren, Y. Chen, and M. Z. Chen, “A variable stiffness soft continuum robot based on pre-charged air, particle jamming, and origami,” in *Proc. IEEE Int. Conf. Robot. Automat.*, 2020, pp. 5869–5875.
- [15] Y. J. Kim, S. Cheng, S. Kim, and K. Iagnemma, “A novel layer jamming mechanism with tunable stiffness capability for minimally invasive surgery,” *IEEE Trans. Robot.*, vol. 29, no. 4, pp. 1031–1042, Aug. 2013.
- [16] Y. Sun et al., “Stiffness customization and patterning for property modulation of silicone-based soft pneumatic actuators,” *Soft Robot.*, vol. 4, no. 3, pp. 251–260, 2017.
- [17] M. E. Giannaccini, C. Xiang, A. Atyabi, T. Theodoridis, S. Nefti-Meziani, and S. Davis, “Novel design of a soft lightweight pneumatic continuum robot arm with decoupled variable stiffness and positioning,” *Soft Robot.*, vol. 5, no. 1, pp. 54–70, 2018.
- [18] J. Y. Lee, W. B. Kim, W. Y. Choi, and K. J. Cho, “Soft robotic blocks: Introducing SoBL, a fast-build modularized design block,” *IEEE Robot. Automat. Mag.*, vol. 23, no. 3, pp. 30–41, Sep. 2016.
- [19] H. Yasuda, T. Yein, T. Tachi, K. Miura, and M. Taya, “Folding behaviour of Tachi-Miura polyhedron bellows,” in *Proc. Roy. Soc. A: Math., Phys. Eng. Sci.*, 2013, vol. 469, no. 2159, Art. no. 20130351.
- [20] S. Li et al., “Scaling up soft robotics: A meter-scale, modular, and reconfigurable soft robotic system,” *Soft Robot.*, vol. 9, no. 2, pp. 324–336, 2022.
- [21] J. L. Silverberg et al., “Using origami design principles to fold re-programmable mechanical metamaterials,” *Science*, vol. 345, no. 6197, pp. 647–650, 2014.
- [22] L. Paez, G. Agarwal, and J. Paik, “Design and analysis of a soft pneumatic actuator with origami shell reinforcement,” *Soft Robot.*, vol. 3, no. 3, pp. 109–119, 2016.
- [23] R. V. Martinez, C. R. Fish, X. Chen, and G. M. Whitesides, “Elastomeric origami: Programmable paper-elastomer composites as pneumatic actuators,” *Adv. Funct. Mater.*, vol. 22, no. 7, pp. 1376–1384, 2012.
- [24] A. R. Deshpande, Z. T. H. Tse, and H. Ren, “Origami-inspired bi-directional soft pneumatic actuator with integrated variable stiffness mechanism,” in *Proc. IEEE 18th Int. Conf. Adv. Robot.*, 2017, pp. 417–421.
- [25] Z. Zhang, G. Chen, H. Wu, L. Kong, and H. Wang, “A pneumatic/cable-driven hybrid linear actuator with combined structure of origami chambers and deployable mechanism,” *IEEE Robot. Automat. Lett.*, vol. 5, no. 2, pp. 3564–3571, Apr. 2020.
- [26] J. G. Lee and H. Rodrigue, “Origami-based vacuum pneumatic artificial muscles with large contraction ratios,” *Soft Robot.*, vol. 6, no. 1, pp. 109–117, 2019.
- [27] T. H. Hong, S. H. Park, J. H. Park, N. J. Paik, and Y. L. Park, “Design of pneumatic origami muscle actuators (POMAs) for a soft robotic hand orthosis for grasping assistance,” in *Proc. IEEE 3rd Int. Conf. Soft Robot.*, 2020, pp. 627–632.
- [28] A. W. Turner, J. P. Kabche, M. L. Peterson, and W. G. Davids, “Tension/torsion testing of inflatable fabric tubes,” *Exp. Techn.*, vol. 32, no. 2, pp. 47–52, 2008.
- [29] W. G. Davids and H. Zhang, “Beam finite element for nonlinear analysis of pressurized fabric beam-columns,” *Eng. Struct.*, vol. 30, no. 7, pp. 1969–1980, 2008.
- [30] Q. T. Nguyen, J. C. Thomas, and A. Le Van, “Inflation and bending of an orthotropic inflatable beam,” *Thin-Walled Struct.*, vol. 88, pp. 129–144, 2015.